Atmospheric
Chemistry
and Physics

Impact of anthropogenic emissions on biogenic secondary organic aerosol: observation in the Pearl River Delta, southern China

Yu-Qing Zhang[1,*], **Duo-Hong Chen**[2,*], **Xiang Ding**[1], **Jun Li**[1], **Tao Zhang**[2], **Jun-Qi Wang**[1], **Qian Cheng**[1], **Hao Jiang**[1],
Wei Song[1], **Yu-Bo Ou**[2], **Peng-Lin Ye**[3], **Gan Zhang**[1], and **Xin-Ming Wang**[1,4]

[1]State Key Laboratory of Organic Geochemistry and Guangdong Provincial Key Laboratory of Environmental Protection and Resources Utilization, Guangzhou Institute of Geochemistry, Chinese Academy of Sciences, Guangzhou 510640, China
[2]State Environmental Protection Key Laboratory of Regional Air Quality Monitoring,
Guangdong Environmental Monitoring Center, Guangzhou 510308, China
[3]Aerodyne Research Inc., Billerica, Massachusetts 01821, USA
[4]Center for Excellence in Regional Atmospheric Environment, Institute of Urban Environment,
Chinese Academy of Sciences, Xiamen 361021, China
*These authors contributed equally to this work.

Correspondence: Xiang Ding (xiangd@gig.ac.cn)

Abstract. Secondary organic aerosol (SOA) formation from biogenic precursors is affected by anthropogenic emissions, which are not well understood in polluted areas. In this study, we accomplished a year-round campaign at nine sites in polluted areas located in the Pearl River Delta (PRD) region during 2015. We measured typical biogenic SOA (BSOA) tracers from isoprene, monoterpenes, and β-caryophyllene, as well as major gaseous and particulate pollutants and investigated the impact of anthropogenic pollutants on BSOA formation. The concentrations of BSOA tracers were in the range of 45.4 to $109\,\mathrm{ng\,m^{-3}}$ with the majority composed of products from monoterpenes (SOA_M, $47.2 \pm 9.29\,\mathrm{ng\,m^{-3}}$), isoprene ($SOA_I$, $23.1 \pm 10.8\,\mathrm{ng\,m^{-3}}$), and β-caryophyllene (SOA_C, $3.85 \pm 1.75\,\mathrm{ng\,m^{-3}}$). We found that atmospheric oxidants, O_x (O_3 plus NO_2), and sulfate correlated well with later-generation SOA_M tracers, but this was not the case for first-generation SOA_M products. This suggested that high O_x and sulfate levels could promote the formation of later-generation SOA_M products, which probably led to the relatively aged SOA_M that we observed in the PRD. For the SOA_I tracers, both 2-methylglyceric acid (NO/NO_2-channel product) and the ratio of 2-methylglyceric acid to 2-methyltetrols (HO_2-channel products) exhibit NO_x dependence, indicating the significant impact of NO_x on SOA_I formation pathways. The SOA_C tracer was elevated in winter

at all sites and was positively correlated with levoglucosan, O_x, and sulfate. Thus, the unexpected increase in SOA_C in wintertime might be highly associated with the enhancement of biomass burning, O_3 chemistry, and the sulfate component in the PRD. The BSOAs that were estimated using the SOA tracer approach showed the highest concentration in fall and the lowest concentration in spring with an annual average concentration of $1.68 \pm 0.40\,\mathrm{\mu g\,m^{-3}}$. SOA_M dominated the BSOA mass all year round. We also found that BSOA correlated well with sulfate and O_x. This implied a significant effect from anthropogenic pollutants on BSOA formation and highlighted that we could reduce BSOA by controlling the anthropogenic emissions of sulfate and O_x precursors in polluted regions.

1 Introduction

Secondary organic aerosols (SOAs) that are produced through homogenous and heterogeneous processes of volatile organic compounds (VOCs) have significant effects on global climate change and regional air quality (Von Schneidemesser et al., 2015). Globally, the emissions of biogenic VOCs (BVOCs) are dominant over anthropogenic VOCs (AVOCs). Thus, biogenic SOA (BSOA) is predomi-

nant with respect to anthropogenic SOA. In the past decade, laboratorial, field, and modeling studies have demonstrated that BSOA formation is highly affected by anthropogenic emissions (Zhang et al., 2015; Hoyle et al., 2011; Carlton et al., 2010). Increasing NO_x shifts isoprene oxidation from low-NO_x conditions to high-NO_x conditions (Surratt et al., 2010) and enhances nighttime SOA formation via nitrate radical oxidation of monoterpenes (Xu et al., 2015). High SO_2 emission leads to abundant sulfate and acidic particles, which accelerate BSOA production due to the "salting-in" effect and acid-catalyzed reactions (Offenberg et al., 2009; Xu et al., 2016). In polluted regions, the increase in O_3 levels due to high emissions of NO_x and VOCs likely results in significant SOA formation via the ozonolysis of BVOCs (Sipilä et al., 2014; Riva et al., 2017). In addition, the large emission and formation of anthropogenic organic matter (OM) in urban areas enhance the incorporation of BVOC oxidation products into the condensed phase (Donahue et al., 2006). Recently, Carlton et al. (2018) found that the removal of anthropogenic emissions of NO_x, SO_2, and primary OA in the Community Multiscale Air Quality Model (CMAQ) simulations could reduce BSOA by 23 %, 14 %, and 8 % in summertime, respectively.

The Pearl River Delta (PRD) region (Fig. 1a) is the most developed area in China. Rapid economic growth in this region during the past 3 decades has resulted in high anthropogenic emissions (Lu et al., 2013). Our observation during the fall–winter season in 2008 at a regional site in the PRD showed that daily $PM_{2.5}$ was as high as $150\,\mu g\,m^{-3}$ (Ding et al., 2012). Fortunately, due to increasingly strict and effective pollution controls in the PRD, $PM_{2.5}$ concentrations have significantly decreased over the last decade and have met the national ambient air quality standard (NAAQS) for annual mean $PM_{2.5}$ ($35\,\mu g\,m^{-3}$) since the year 2015 (Figure 1b). However, O_3 and oxidant species (O_x, $O_x = O_3 + NO_2$) are still at high levels and have shown no apparent decrease (Fig. 1b). Hofzumahaus et al. (2009) observed extremely high OH concentrations in the PRD and proposed a recycling mechanism that increases the stability of OH in the air of polluted regions. All of the abovementioned results indicate a high atmospheric oxidative capacity in the PRD, as O_3, NO_x, and OH are intimately linked in atmospheric chemistry. Moreover, BVOC emissions in the PRD are expected to be high year-round due to the area's subtropical climate (Zheng et al., 2010). During the process of such dramatic changes in air pollution characteristics (e.g., $PM_{2.5}$ and O_3), BSOA origins and formation mechanisms in the PRD should have been profoundly affected over the last decade.

In this study, year-round $PM_{2.5}$ samples were collected at nine sites in the PRD during 2015. We investigated SOA tracers from typical BVOCs (isoprene, monoterpenes, and β-caryophyllene) across the PRD for the first time. We checked seasonal variations in the concentrations and compositions of these BSOA tracers and evaluated the impact of anthropogenic pollutants on BSOA formation in the PRD. We also
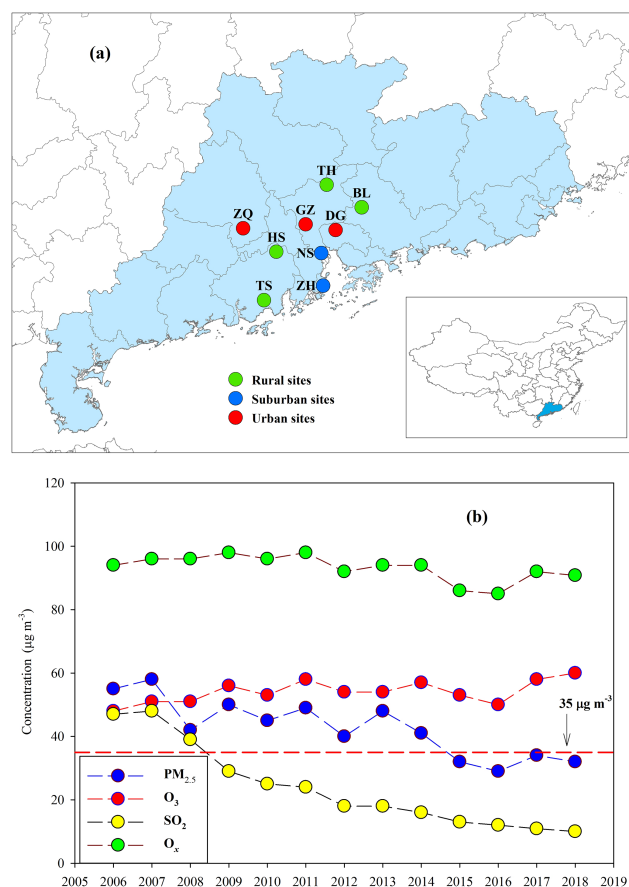

Figure 1. (a) Sampling sites in the PRD, including Zhaoqing (ZQ), Guangzhou (GZ), Dongguan (DG), Nansha (NS), Zhuhai (ZH), Tianhu (TH), Boluo (BL), Heshan (HS), and Taishan (TS), and **(b)** long-term trends of annual mean $PM_{2.5}$, O_3, SO_2, and O_x recorded by the Guangdong–Hong Kong–Macao regional air quality monitoring network (http://gdee.gd.gov.cn/kqjc/, last access: 26 November 2019) . The red dashed line indicates the NAAQS for annual mean $PM_{2.5}$ concentrations ($35\,\mu g\,m^{-3}$).

accessed the SOA origins and discussed the possibility of further reducing BSOA by controlling anthropogenic emissions.

2 Experimental section

2.1 Field sampling

Concurrent sampling was performed at 9 of the 23 Guangdong–Hong Kong–Macao regional air quality monitoring network sites (http://gdee.gd.gov.cn/kqjc/, last access: 26 November 2019, Fig. 1a), including 3 urban sites in Zhaoqing (ZQ), Guangzhou (GZ), and Dongguan (DG); 2 suburban sites in Nansha (NS) and Zhuhai (ZH); and 4 rural sites in Tianhu (TH), Boluo (BL), Heshan (HS), and Taishan (TS).

At each site, 24 h sampling was conducted every 6 d from January to December in 2015 using a $PM_{2.5}$ sampler equipped with quartz filters (8 in. × 10 in.) at a flow rate of

1.1 m^3 min^{-1}. Additionally, field blanks were collected at all sites at a monthly interval. Blank filters were covered with aluminum foil, baked at 500 °C for 12 h, and stored in a container with silica gel. After sampling, the filter samples were stored at −20 °C.

In this study, the filters collected in January, April, July, and October 2015 were selected to represent winter, spring, summer, and fall, respectively. A total of 170 field samples (4–5 samples for each season at each site) were analyzed in the current study.

2.2 Chemical analysis

For each filter, organic carbon (OC) and elemental carbon (EC) were measured using an OC–EC aerosol analyzer (Sunset Laboratory Inc.). Water-soluble ions were analyzed by ion chromatography (Metrohm). All of these species are major components in PM$_{2.5}$ (see Fig. 2). Meteorological parameters (temperature and relative humidity) and gaseous pollutants (SO$_2$, CO, NO$_2$, NO, and O$_3$) at each site were recorded hourly. We also calculated the daily averages to probe the potential influence of air pollutants on BSOA formation.

For BSOA tracer analysis, detailed information regarding the processes used is given in the existing literature (Shen et al., 2015; Ding et al., 2012). Isotope-labeled standard mixtures, including dodecanoic acid-d$_{23}$, hexadecanoic acid-d$_{31}$, docosanoic acid-d$_{43}$, and levoglucosan-^{13}C$_6$ were added into each sample as internal standards. Samples were then extracted by sonication with the mixed solvents of dichloride methane (DCM)/hexane (1 : 1, v/v) and DCM/methanol (1 : 1, v/v), sequentially. The extraction solutions of each sample were combined, filtered, and concentrated to ∼ 2 mL. Each concentrated sample was split into two parts for silylation and methylation, respectively.

We analyzed 14 BSOA tracers in the derivatized samples using GC-MSD (Agilent 7890/5975C). The isoprene-derived SOA (SOA$_I$) tracers were composed of 2-methyltetrols (2-MTLs, 2-methylthreitol, and 2-methylerythritol) (Claeys et al., 2004a), 2-methylglyceric acid (2-MGA) (Claeys et al., 2004b), 3-MeTHF-3,4-diols (*cis*-3-methyltetrahydrofuran-3,4-diol and *trans*-3-methyltetrahydrofuran-3,4-diol) (Lin et al., 2012), and C$_5$-alkene triols (*cis*-2-methyl-1,3,4-trihydroxy-1-butene, *trans*-2-methyl-1,3,4-trihydroxy-1-butene, and 3-methyl-2,3,4-trihydroxy-1-butene) (Wang et al., 2005). The monoterpene-derived SOA (SOA$_M$) tracers included 3-hydroxy-4,4-dimethylglutaric acid (HDMGA), 3-hydroxyglutaric acid (HGA) (Claeys et al., 2007), pinic acid (PA), *cis*-pinonic acid (PNA) (Christoffersen et al., 1998), and 3-methyl-1,2,3-butanetricarboxylic acid (MBTCA) (Szmigielski et al., 2007). The β-caryophyllene-derived SOA (SOA$_C$) tracer was β-caryophyllenic acid (CA) (Jaoui et al., 2007). Due to the lack of authentic standards, surrogate standards were used to quantify BSOA tracers except PNA. Specifically, erythritol, PNA, and octadecanoic acid were used for the quantification of SOA$_I$ tracers (Ding et al., 2008), other SOA$_M$ tracers (Ding et al., 2014), and CA (Ding et al., 2011), respectively. The method detection limits (MDLs) for erythritol, PNA, and octadecanoic acid were 0.01, 0.02, and 0.02 ng m^{-3}, respectively. Table S1 in the Supplement summarizes BSOA data from each site in the PRD.

2.3 Quality assurance/quality control

The target BSOA tracers were not detected or were lower than the MDLs in the field blanks. The results of spiked samples (erythritol-, PNA-, and octadecanoic-acid-spiked in prebaked quartz filters) indicated that the recoveries were 65 % ±14 % for erythritol, 101 % ±3 % for PNA, and 83 % ±7 % for octadecanoic acid. The results of paired duplicate samples indicated that all of the relative differences for target BSOA tracers were lower than 15 %.

It should be noted that the application of surrogate quantification introduces additional errors to the results. Based on the empirical approach of calculating uncertainties from surrogate quantification (Stone et al., 2012), we estimated the errors in analyte measurement that were propagated from the uncertainties in field blanks, spike recoveries, repeatability, and surrogate quantification. As Table S2 shows, the estimated uncertainties in the tracers' measurement ranged from 15 % (PNA) to 157 % (CA).

3 Results and discussion

3.1 PM$_{2.5}$ and gaseous pollutants

Figure 2 presents the spatial and seasonal variations of PM$_{2.5}$ and its major components. Although annual mean PM$_{2.5}$ (34.8 ± 6.1 µg m^{-3}) in the PRD met the NAAQS value of 35 µg m^{-3}, PM$_{2.5}$ concentrations at the urban sites (ZQ, GZ, and DG) all exceeded the NAAQS value. The rural TH site in the northern part of the PRD witnessed the lowest PM$_{2.5}$ concentration (25.0 µg m^{-3}) among the nine sites. PM$_{2.5}$ levels were highest in winter (60.1 ± 21.6 µg m^{-3} on average) and lowest in summer (22.8 ± 3.3 µg m^{-3} on average). Carbonaceous aerosols and water-soluble ions together explained 98 % ±11 % of the PM$_{2.5}$ mass. OM (OC × 1.6) was the most abundant component in PM$_{2.5}$, followed by sulfate, ammonium, nitrate, and EC. Similar to PM$_{2.5}$, the five major components all increased in winter and fall (Fig. S1), suggesting severe PM$_{2.5}$ pollution during the fall–winter season in the PRD.

In the gas phase, SO$_2$, CO, NO$_2$, and NO$_x$ presented similar seasonal trends to PM$_{2.5}$; i.e., higher levels occurred during fall and winter and lower concentrations during spring and summer (Fig. 3a, b, c, d). Annual mean SO$_2$ and NO$_2$ in the PRD both met the NAAQS values of 60 and 40 µg m^{-3}, respectively (Fig. 3a, c). As a typical secondary pollutant, O$_3$ was highest in summer (Fig. 3e), probably due to the strong photochemistry. Due to the compromise of opposite seasonal
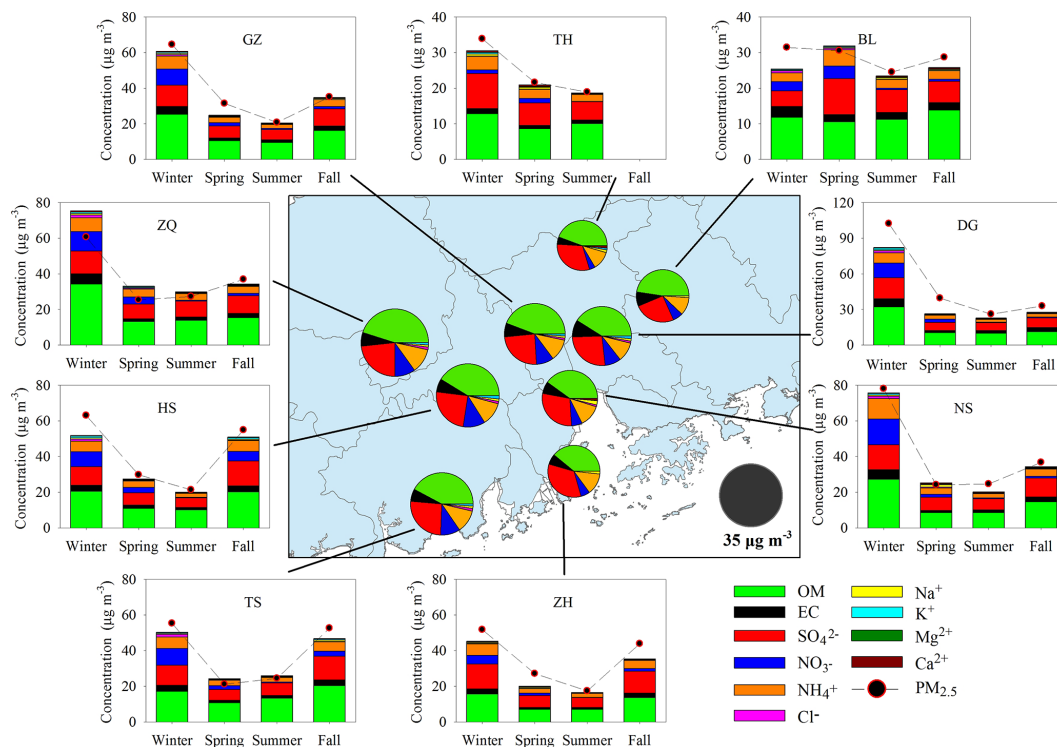
Figure 2. Major components in $PM_{2.5}$ and their seasonal variation at nine sites. The pie charts in the central panel represent the annual average of the major components. High levels of $PM_{2.5}$ and major components were observed in wintertime.

trends of O_3 and NO_2, O_x showed less seasonal variation (Fig. 3f) compared with other gaseous pollutants, and the annual mean for O_x reached $96.1 \pm 14.9\,\mu g\,m^{-3}$. This indicated significant year-round O_3 pollution in the PRD.

3.2 Spatial distribution and seasonal variation of SOA tracers

The total concentrations of BSOA tracers ranged from 45.4 to $109\,ng\,m^{-3}$ among the nine sites. SOA_M tracers ($47.2 \pm 9.29\,ng\,m^{-3}$) were predominant, followed by SOA_I tracers ($23.1 \pm 10.8\,ng\,m^{-3}$) and SOA_C tracers ($3.85 \pm 1.75\,ng\,m^{-3}$).

3.2.1 Monoterpene-derived SOA tracers

Annual averages of total SOA_M tracers at the nine sites were in the range of 26.5 to $57.4\,ng\,m^{-3}$ (Table S1). Figures 4 and S2a show the spatial distribution of SOA_M tracers and monoterpene emissions in the PRD (Zheng et al., 2010). The highest concentration of SOA_M tracers was observed at the rural TH site, where monoterpene emissions were high. Figure 4 also presents seasonal variations of SOA_M tracers. At most sites, high levels occurred in summer and fall. Monoterpene emission rates are influenced by temperature and solar radiation (Guenther et al., 2012). Thus, high temperature and intensive solar radiation during summer and fall in the PRD

(Zheng et al., 2010) could stimulate monoterpene emissions and subsequent SOA_M formation.

Among the five SOA_M tracers, HGA ($20.1 \pm 4.28\,ng\,m^{-3}$) showed the highest concentration, followed by HDMGA ($14.7 \pm 2.93\,ng\,m^{-3}$), MBTCA ($7.63 \pm 1.49\,ng\,m^{-3}$), PNA ($3.75 \pm 2.72\,ng\,m^{-3}$), and PA ($1.01 \pm 0.48\,ng\,m^{-3}$). SOA_M formation undergoes multigenerational reactions. The first-generation SOA_M (SOA_{M_F}) products, PNA and PA, can be further oxidized and form the later-generation (SOA_{M_L}) products, e.g., MBTCA (Müller et al., 2012). Thus, the (PNA + PA) / MBTCA ratio has been used to probe SOA_M aging (Haque et al., 2016; Ding et al., 2014). The (PNA + PA) / MBTCA ratios in chamber-generated α-pinene SOA samples were reported to be in the range of 1.51 to 5.91, depending on different oxidation conditions (Offenberg et al., 2007; Eddingsaas et al., 2012). In this study, the median values of (PNA + PA) / MBTCA varied from 0.27 at ZH to 1.67 at TH. The ratios observed in this study were consistent with our previous observations at the regional site, Wanqingsha (WQS) in the PRD (Ding et al., 2012), but lower than those in fresh α-pinene SOA samples from chamber experiments (Fig. S3), indicating relatively aged SOA_M in the air of the PRD.

Moreover, the levels of SOA_{M_L} tracers (HGA + HDMGA + MBTCA) were much higher than those of SOA_{M_F} tracers (PNA + PA), with mean mass fractions of SOA_{M_L} tracers reaching 86 % (Fig. 4). Mass
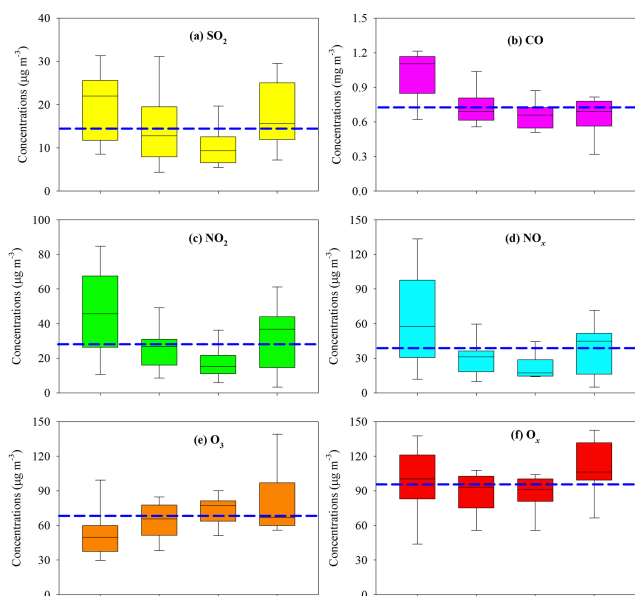
Figure 3. Seasonal variation of gaseous pollutants in the PRD. The boxes with error bars represent the 10th, 25th, 75th, and 90th percentiles for each pollutant. The line in each box represents the median value. The blue dashed lines indicate the annual average concentrations of SO_2 ($14.9 \, \mu g \, m^{-3}$), CO ($0.74 \, mg \, m^{-3}$), NO_2 ($28.5 \, \mu g \, m^{-3}$), NO_x ($39.0 \, \mu g \, m^{-3}$), O_3 ($67.7 \, \mu g \, m^{-3}$), and O_x ($96.1 \, \mu g \, m^{-3}$).

fractions of SOA_{M_F} tracers decreased in the summer samples (Fig. 4), probably resulting from strong photochemistry and more intensive subsequent oxidation during summer. High abundances of SOA_{M_L} tracers in the PRD were different from our year-round observations at 12 sites across China (Ding et al., 2016b). Ding et al. (2016b) found that the $(PNA + PA)/MBTCA$ ratio suggested generally fresh SOA_M (Fig. S3) and that SOA_{M_F} tracers were predominant. Thus, we see more aged SOA_M in the PRD.

As Figs. 5a–b, S4, and S5 show, the SOA_{M_F} tracers did not show good correlations with O_x at most sites, whereas the SOA_{M_L} tracers exhibited significant O_x dependence. When O_x is high, strong photooxidation of PNA and PA could reduce their concentrations and promote the formation of SOA_{M_L} tracers (Müller et al., 2012). Thus, the levels of SOA_{M_L} tracers would increase with increasing O_x, whereas this is not the case for SOA_{M_F} tracers. Moreover, sulfate could influence SOA formation. Sulfate is a key species in particles that determines the aerosol liquid water amount, aerosol acidity, and particle surface area (Xu et al., 2015, 2016). Thus, an increase in sulfate could promote aqueous and heterogeneous reactions. In this study, the SOA_{M_F} tracers poorly correlated with sulfate (Fig. 5c), whereas the SOA_{M_L} tracers positively correlated with sulfate at all nine sites (Fig. 5d). At each site, the SOA_{M_L} tracers exhibited more sulfate dependence than the SOA_{M_F} tracers (Fig. S5). This suggested that sulfate also played a critical role in form-

ing SOA_{M_L} tracers through particle-phase reactions. In addition to gas-phase OH oxidation (Müller et al., 2012), the heterogeneous OH oxidation of PNA could also produce SOA_{M_L} tracers (Lai et al., 2015). Aljawhary et al. (2016) reported the kinetics and mechanism of PNA oxidation in acidic solutions and found that the molar yields of MBTCA via aqueous-phase reactions were similar to those in gas-phase oxidation. Here, we conclude that high concentrations of O_x and sulfate could stimulate SOA_{M_L} tracer production and thereby lead to aged SOA_M in the PRD.

3.2.2 Isoprene-derived SOA tracers

Annual averages of total SOA_I tracers at the nine sites were in the range of 10.8 to $49.3 \, ng \, m^{-3}$ (Table S1). Figures 6 and S2b show the spatial distribution of SOA_I tracers and isoprene emissions in the PRD (Zheng et al., 2010), respectively. The highest concentration occurred at ZQ, where emissions were high. Figure 6 also presents seasonal variations of SOA_I tracers at the nine sites. High levels occurred in summer and fall. Similar to monoterpenes, the emission rate of isoprene is influenced by temperature and solar radiation (Guenther et al., 2012), which are both expected to be higher in summer and fall in the PRD (Zheng et al., 2010). Among these SOA_I tracers, 2-MTLs ($14.2 \pm 5.61 \, ng \, m^{-3}$) were the most abundant products, followed by C_5-alkene triols ($6.81 \pm 5.05 \, ng \, m^{-3}$), 2-MGA ($1.99 \pm 0.72 \, ng \, m^{-3}$), and 3-MeTHF-3,4-diols ($0.19 \pm 0.08 \, ng \, m^{-3}$).

SOA_I formation is highly affected by NO_x (Surratt et al., 2010). Under low-NO_x or NO_x-free conditions, isoprene is oxidized by the OH and HO_2 radicals via the HO_2 channel which generates a hydroxy hydroperoxide (ISOPOOH) and then forms epoxydiols (IEPOX) (Paulot et al., 2009). Reactive uptake of IEPOX on acidic particles eventually produces 2-MTLs, C_5-alkene triols, 3-MeTHF-3,4-diols, 2-MTLs-organosulfates, and oligomers (Lin et al., 2012). Under high-NO_x conditions, isoprene undergoes oxidation by NO_x via the NO/NO_2 channel, generates methacrolein (MACR), and then forms peroxymethylacrylic nitric anhydride (MPAN). Further oxidation of MPAN by the OH radical produces hydroxymethyl-methyl-α-lactone (HMML) and/or methacrylic acid epoxide (MAE). HMML and MAE are the direct precursors of 2-MGA, 2-MGA-organosulfate, and its corresponding oligomers (Nguyen et al., 2015). As Fig. 6 shows, the concentrations of HO_2-channel tracers (2-MTLs + C_5-alkene triols + 3-MeTHF-3,4-diols) were much higher than those of the NO/NO_2-channel product (2-MGA) at all the nine sites. The dominance of HO_2-channel products was also observed at another regional site (WQS) in the PRD (He et al., 2018).

Figure 6 also shows seasonal trends of the 2-MGA to 2-MTLs ratio (2-MGA/2-MTLs) which is often applied to probe the influence of NO_x on the formation of SOA_I (Ding et al., 2013, 2016a; Pye et al., 2013). The ratios were highest in wintertime and lowest in summertime; these results are
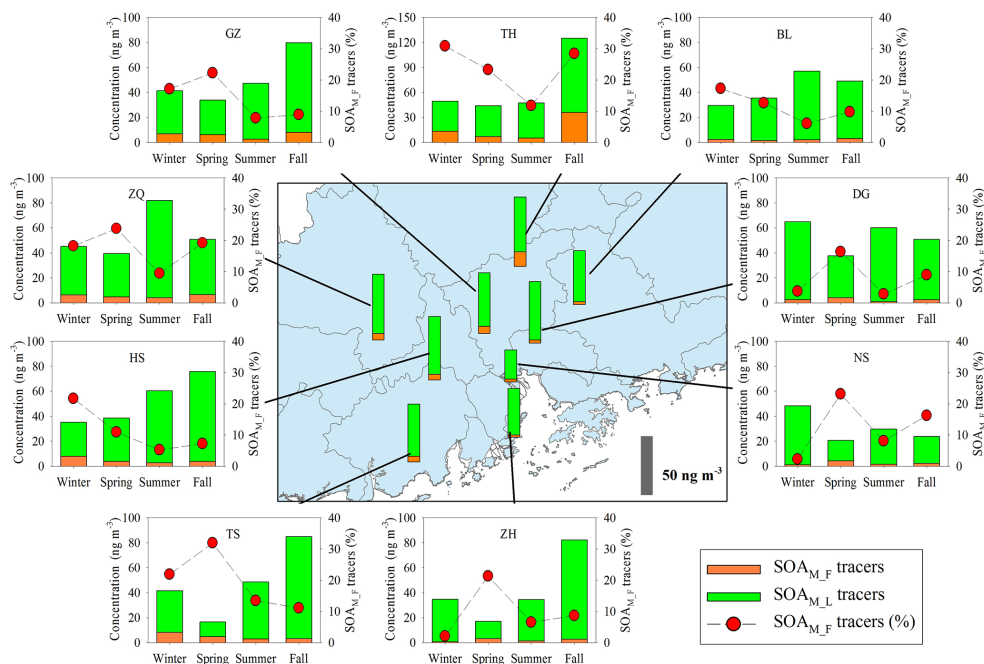
Figure 4. Spatial and seasonal variations of SOA_M tracers at nine sites in the PRD. The bars in the central panel represent the annual average concentrations of the SOA_M tracers.
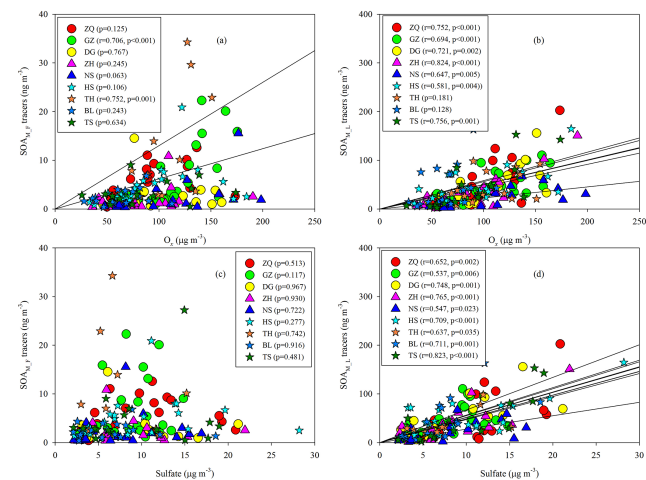

Figure 5. Correlations of SOA_{M_F} and SOA_{M_L} tracers with O_x **(a, b)** and sulfate **(c, d)**.

Table 1. Correlations between SOA_I tracers and NO_x.

| | 2-MGA | | 2-MGA/2-MTLs | |
	Coeffi-cient (r)	p value	Coeffi-cient (r)	p value
NO	0.028	0.733	0.166	0.043
NO_2	0.205	0.008	0.352	< 0.001
NO_x	0.132	0.102	0.286	< 0.001
NO_2/NO	0.001	0.986	0.162	0.048

the 2-MGA/2-MTLs ratio correlated well with NO, NO_2, and the NO_2/NO ratio (Table 1). Increasing NO limits the formation of ISOPOOH but prefers the production of MACR, and increasing NO_2 enhances MPAN formation. Thus, it is expected that the 2-MGA/2-MTLs ratio will show stronger NO_x dependence than 2-MGA. These findings demonstrate the significant impact of NO_x on SOA_I formation pathways in the atmosphere. We also checked the correlations of SOA_I tracers with O_x and sulfate (Fig. S6). The NO/NO_2-channel product exhibited more O_x and sulfate dependance than the HO_2-channel products.

Recent studies have indicated that isoprene ozonolysis might play a role in SOA_I formation in the ambient air. Riva et al. (2016) found that isoprene ozonolysis with acidic particles could produce substantial 2-MTLs, but this was not the case for C_5-alkene triols and 3-MeTHF-3,4-diols. Li et al. (2018) observed a positive correlation between 2-MTLs and O_3 on the North China Plain. In the PRD, we also saw
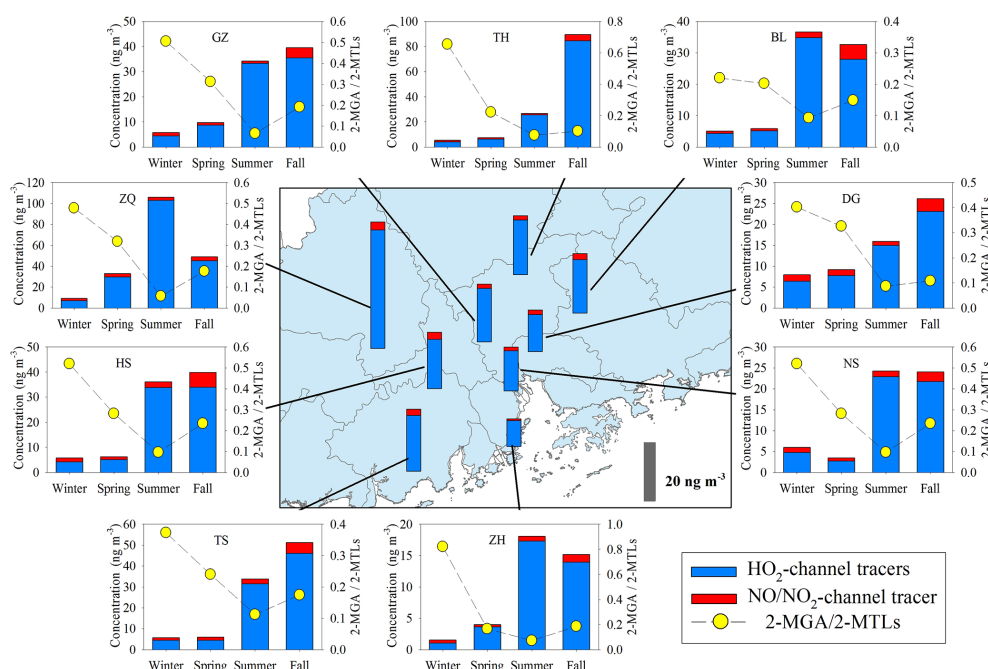
consistent with the seasonal trend of NO_x during our campaign (Fig. 3d). As Table 1 shows, 2-MGA was positively correlated with NO_2, probably due to the enhanced formation of MPAN from the peroxymethacryoyl (PMA) radical which reacted with NO_2 (Worton et al., 2013; Chan et al., 2010). Previous laboratory studies have shown that increasing the NO_2/NO ratio could promote the formation of 2-MGA and its corresponding oligoesters (Chan et al., 2010; Surratt et al., 2010). However, we did not see a significant correlation between 2-MGA and the NO_2/NO ratio in the PRD. Instead,

Figure 6. Spatial and seasonal variations of SOA$_I$ tracers at nine sites in the PRD. The bars in the central panel represent the annual average concentrations of the SOA$_I$ tracers.
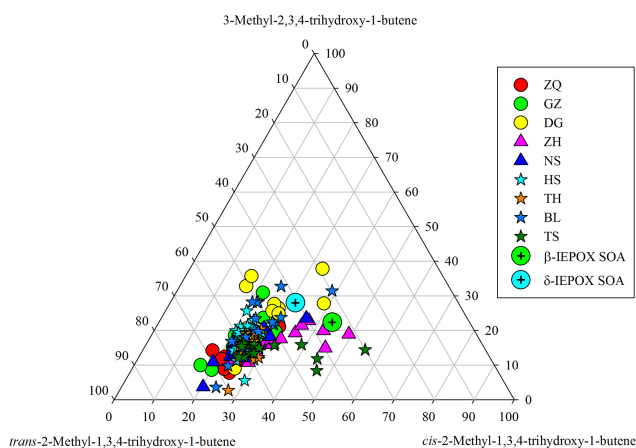

Figure 7. Ternary plot of C$_5$-alkene triol isomers in the PRD samples and in the β-IEPOX- and δ-IEPOX-derived SOA (Lin et al., 2012).

weak but significant correlations of 2-MTLs with O$_3$ (Table S3). However, 3-MeTHF-3,4-diols and C$_5$-alkene triols were detected in all samples, and 2-MTLs, C$_5$-alkene triols, and 3-MeTHF-3,4-diols correlated well with each other (Table S4), which was apparently different from the results reported by Riva et al. (2016). Moreover, the ratios of 2-MTLs isomers in the PRD samples (2.00–2.85) were much lower than those (10–22; Fig. S7) reported in the SOA from isoprene ozonolysis (Riva et al., 2016). Furthermore, isoprene oxidation by the OH radical is much faster than oxidation by

O$_3$ under polluted PRD conditions (Table S5), and IEPOX yields via ISOPOOH oxidation by the OH radical are more than 75% in the atmosphere (St. Clair et al., 2016). Thus, isoprene ozonolysis might be not the major formation pathway of SOA$_I$, even though the annual mean O$_3$ level reached 67.7 µg m^{-3} in the PRD (Table S1).

Previous studies have found that thermal decomposition of low-volatility organics in IEPOX-derived SOA could produce SOA$_I$ tracers, e.g., 2-MTLs, C$_5$-alkene triols, and 3-MeTHF-3,4-diols (Lopez-Hilfiker et al., 2016; Watanabe et al., 2018). This means that these tracers detected by GC-MSD might be generated from the thermal decomposition of IEPOX-derived SOA. As estimated by Cui et al. (2018), 14.7 %–42.8 % of C$_5$-alkene triols, 11.1 % of 2-MTLs, and approximately all 3-MeTHF-3,4-diols measured by GC-MSD could be attributed to the thermal degradation of 2-MTL-derived organosulfates (MTL-OSs). We also measured MTL-OSs in two samples at the HS and TS sites (Table S6), respectively, utilizing the widely used LC-MS approach (He et al., 2014, 2018). Assuming that all MTL-OSs decomposed to these tracers, the thermal decomposition of MTL-OSs would account for 15.1 %–31.6 % of C$_5$-alkene triols, 6.0 %–10.0 % of 2-MTLs, and all 3-MeTHF-3,4-diols measured by GC/MSD. Thus, C$_5$-alkene triols and 2-MTLs are major products of isoprene oxidation rather than products of the thermal decomposition of MTL-OSs, whereas 3-MeTHF-3,4-diols are only present in trace amount in the air and might be produced largely from thermal degradation.
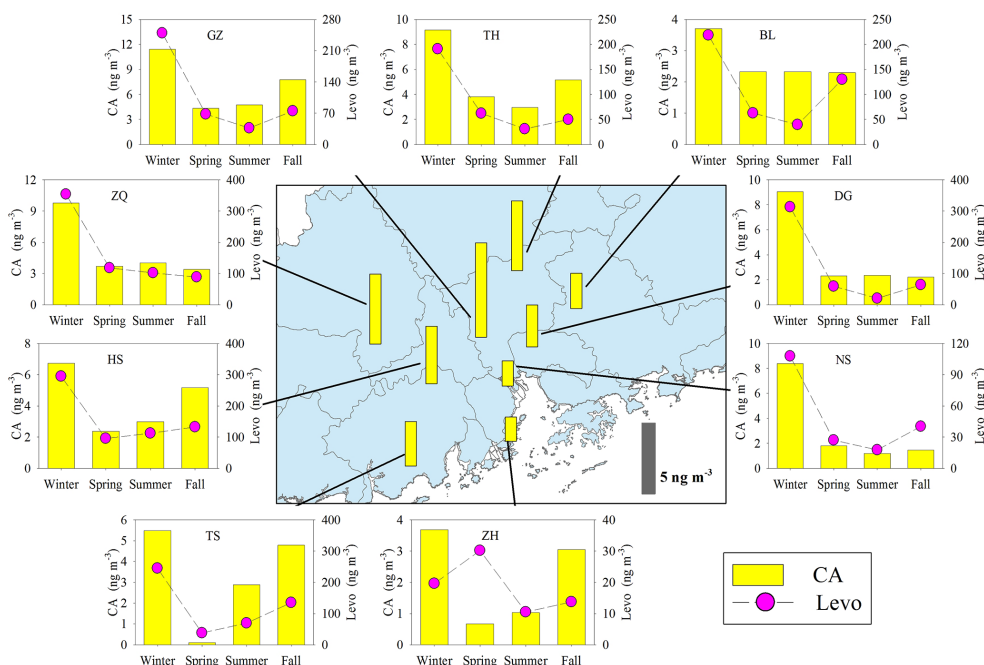
Figure 8. Spatial and seasonal variations of SOA$_C$ tracer (CA) at nine sites in the PRD. The bars in the central panel represent the annual average concentration of the SOA$_C$ tracers. The pink circle indicates the BB tracer, levoglucosan (Levo).

Moreover, we see significant variations in SOA$_I$ tracer compositions in the PRD. For instance, C$_5$-alkene triols have three isomers. If these tracers were mainly generated from a thermal process, their compositions should be similar in different samples. In fact, the relative abundances of the three C$_5$-alkene triol isomers significantly changed from site to site (Fig. 7) and from season to season (Fig. S8), and their compositions in the PRD were different from those measured in the chamber samples (Lin et al., 2012). In addition, the slopes of linear correlations among these IEPOX-derived SOA tracers also varied from site to site (Fig. S9). Coupled with the seasonal trend of 2-MGA/2-MTLs ratios, the apparent variations in SOA$_I$ tracer compositions demonstrate that these SOA$_I$ tracers are mainly formed via different pathways in the ambient atmosphere; however, they might partly arise from the thermal decomposition of different dimers/OSs, and the parent dimers/OSs vary with site and seasons.

3.2.3 Sesquiterpene-derived SOA tracer

Annual averages of CA at the nine sites ranged from 1.82 to 7.07 ng m^{-3}. The levels of CA at the inland sites (e.g., GZ, ZQ, and TH) were higher than those at the coastal sites (ZH and NS; Fig. 8). As sesquiterpenes are typical BVOCs, it is unexpected that the concentrations of CA were highest during winter in the PRD (Fig. 8). Interestingly, the seasonal trend of CA was consistent with that of the biomass burning (BB) tracer, levoglucosan (Fig. 8), and CA correlated well with levoglucosan at eight sites in the PRD (Fig. 9a). Sesquiterpenes are stored in plant tissues, partly to protect the

plants from insects and pathogens (Keeling and Bohlmann, 2006). BB can not only stimulate sesquiterpene emissions (Ciccioli et al., 2014) but can also substantially alter SOA formation and yields (Mentel et al., 2013). Emissions inventories in the PRD showed that BB emissions were enhanced during winter (He et al., 2011). This suggested that the unexpected increase in SOA$_C$ in wintertime could be highly associated with BB emissions in the PRD.

Besides the impact of BB, we also found positive correlations of CA with O$_x$ (Fig. 9b) and sulfate (Fig. 9c). The oxidation of β-caryophyllene by the OH radical and O$_3$ is very rapid. Under typical oxidation conditions in the air of the PRD, the lifetimes of β-caryophyllene are only several minutes (Table S5). Once emitted from vegetation or biomass burning, β-caryophyllene will react rapidly and form CA immediately. This partly explains the positive correlations between CA and levoglucosan in this region. The unexpected high levels of CA in the winter indicated that biomass burning could be an important source of SOA$_C$ in the PRD, especially in wintertime. In addition, the increase in sulfate could raise aerosol acidity and thereby promote aqueous and heterogeneous reactions to form SOA$_C$. In the PRD, both O$_x$ (Fig. 3f) and sulfate (Fig. S1) increased during winter, which could promote SOA$_C$ formation. Here, we conclude that the enhancement of BB emissions as well as the increase in O$_x$ and sulfate in wintertime led to high SOA$_C$ production during this season in the PRD.
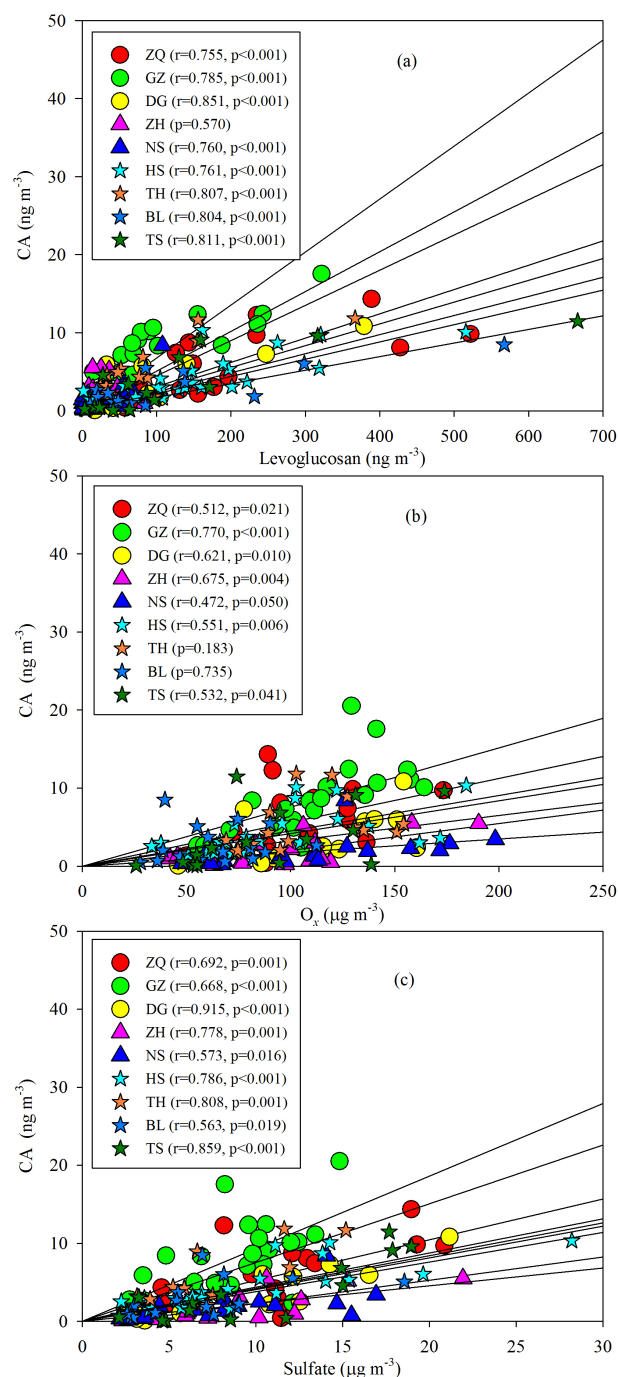
Figure 9. Significant correlations of CA with levoglucosan **(a)**, O_x **(b)**, and sulfate **(c)**.

3.3 Source apportionment and atmospheric implications

We further attributed BSOA using the SOA tracer approach, which was first developed by Kleindienst et al. (2007). This method has been applied to SOA apportionment at multiple sites across the United States (Lewandowski et al., 2013)
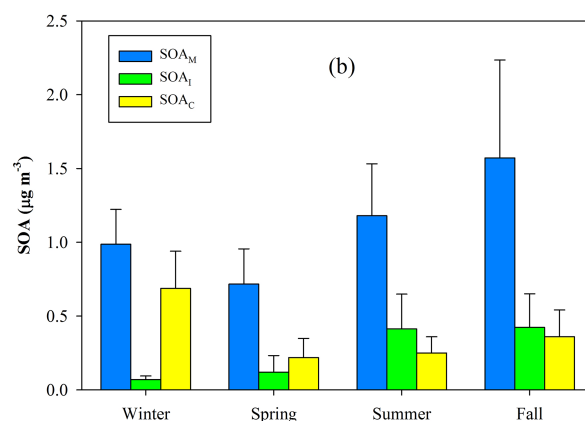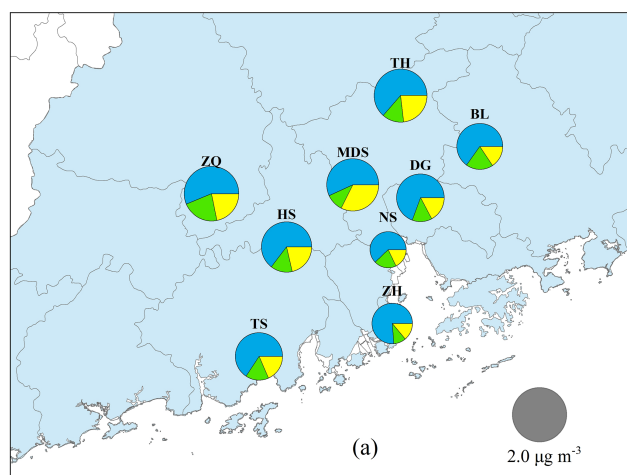

Figure 10. Spatial **(a)** and seasonal **(b)** variations in BSOA components.

and China (Ding et al., 2016b), and over global oceans from the Arctic to the Antarctic (Hu et al., 2013). Details of the SOA tracer method and its application in this study as well as the uncertainty of the estimation procedure are described in Sect. S1. Table S1 lists the results of estimated SOAs from different BVOCs.

Figure 10a exhibits the spatial distribution of BSOA components ($SOA_M + SOA_I + SOA_C$). The annual average at the nine sites ranged from $0.97\,\mu\mathrm{g\,m^{-3}}$ (NS) to $2.19\,\mu\mathrm{g\,m^{-3}}$ (ZQ), accounting for 9 %–15 % of OM. SOA_M was the largest BSOA contributor with an average contribution of 64 % ±7 %, followed by SOA_C (21 % ±6 %), and SOA_I (14 % ±4 %). Figure 10b presents the seasonal variation of BSOA components. The levels were highest in fall ($2.35 \pm 0.95\,\mu\mathrm{g\,m^{-3}}$) and lowest in spring ($1.06 \pm 0.42\,\mu\mathrm{g\,m^{-3}}$). SOA_M contributions ranged from 57 % in winter to 68 % in spring. The contribution of SOA_I was only 5 % in winter and reached up to 22 % in summer. The contribution of SOA_C increased to 40 % in wintertime.

Table 2. Correlations of BSOA with sulfate and O_x.

	Sulfate			O_x		
	Slope	p value	%[a]	Slope	p value	%[a]
SOA_M	0.112	< 0.001	45	0.013	< 0.001	57
SOA_I	0.020	< 0.001	34	0.003	< 0.001	50
SOA_C	0.041	< 0.001	46	0.004	< 0.001	55
BSOA	0.172	< 0.001	44	0.019	< 0.001	55

[a] Percentage reduction of SOA due to a 50 % decline in sulfate or O_x.

It is interesting to note that SOA_M, SOA_I, and SOA_C all positively correlated with sulfate and O_x in the PRD (Table 2). As anthropogenic emissions can enhance BSOA formation (Hoyle et al., 2011), the reduction of anthropogenic emissions indeed lowers BSOA production (Carlton et al., 2018). As the oxidation product of SO_2, sulfate is a key species in particles and determines aerosol acidity and surface area (Xu et al., 2015, 2016); thus, sulfate could promote BSOA formation via acid-catalyzed heterogeneous reactions. A recent study found that SO_2 could directly react with organic peroxides from monoterpene ozonolysis and form substantial organosulfates (Ye et al., 2018). Thus, a decrease in SO_2 emissions indeed reduces SO_2 and sulfate in the ambient air, which leads to less acidic particles and a reduction in BSOA production. For O_x, the increase in O_3 likely results in significant SOA formation via BVOC ozonolysis (Sipilä et al., 2014; Riva et al., 2017). Hence, the decrease in O_x resulting from the control of VOC and NO_x emissions could reduce BSOA formation through O_3 chemistry. Based on the observed sulfate and O_x dependence of BSOA in this study, a reduction of 1 µg m^{-3} in sulfate and O_x in the air of the PRD could lower BSOA levels by 0.17 and 0.02 µg m^{-3}, respectively. If both concentrations decline by 50 %, the reduction of O_x is more efficient than the reduction of sulfate with respect to reducing BSOA in the PRD (Table 2).

We further compared the results from 2015 with those from the fall–winter season of 2008 at WQS (Ding et al., 2012). We found that all BSOA species positively correlated with sulfate but exhibited no O_x dependence (Table S7). Thus, BSOA formation was largely influenced by sulfate in 2008, probably due to high sulfate levels during this period (as high as 46.8 µg m^{-3}). Owing to subsequent strict control of SO_2 emissions (Wang et al., 2013), ambient SO_2 has significantly decreased over the PRD (Fig. 1b). Our long-term observation during the fall–winter season at WQS also witnessed a decreasing trend in sulfate from 2007 to 2016 (Fig. S10). However, O_x levels have not decreased during the past decade (Fig. 1b), and O_x concentrations were much higher than sulfate in 2015 in the PRD (96.1 ± 14.9 µg m^{-3} vs. 8.44 ± 1.09 µg m^{-3} on average). These results emphasize the current importance of O_x in BSOA formation in the PRD. At present, short-term despiking and long-term attainment of O_3 concentrations are challenges for air pollution control in the PRD (Ou et al., 2016). Thus, lowering O_x is critical to improve the air quality in the PRD. Our results highlight the importance of future reductions of anthropogenic pollutant emissions (e.g., SO_2 and O_x precursors) in order to considerably reduce the BSOA burden in polluted regions.

References

Aljawhary, D., Zhao, R., Lee, A. K. Y., Wang, C., and Abbatt, J. P. D.: Kinetics, mechanism, and secondary organic aerosol yield of aqueous phase photo-oxidation of α-pinene oxidation products, J. Phys. Chem. A., 120, 1395–1407, https://doi.org/10.1021/acs.jpca.5b06237, 2016.

Carlton, A. G., Pinder, R. W., Bhave, P. V., and Pouliot, G. A.: To what extent can biogenic SOA be controlled?, Environ. Sci. Technol., 44, 3376–3380, https://doi.org/10.1021/es903506b, 2010.

Carlton, A. G., Pye, H. O. T., Baker, K. R., and Hennigan, C. J.: Additional benefits of federal air-quality rules: Model estimates of controllable biogenic secondary organic aerosol, Environ. Sci. Technol., 52, 9254–9265, https://doi.org/10.1021/acs.est.8b01869, 2018.

Chan, A. W. H., Chan, M. N., Surratt, J. D., Chhabra, P. S., Loza, C. L., Crounse, J. D., Yee, L. D., Flagan, R. C., Wennberg, P. O., and Seinfeld, J. H.: Role of aldehyde chemistry and NOx concentrations in secondary organic aerosol formation, Atmos. Chem. Phys., 10, 7169–7188, https://doi.org/10.5194/acp-10-7169-2010, 2010.

Christoffersen, T. S., Hjorth, J., Horie, O., Jensen, N. R., Kotzias, D., Molander, L. L., Neeb, P., Ruppert, L., Winterhalter, R., Virkkula, A., Wirtz, K., and Larsen, B. R.: Cispinic acid, a possible precursor for organic aerosol formation from ozonolysis of α-pinene, Atmos. Environ., 32, 1657–1661, https://doi.org/10.1016/S1352-2310(97)00448-2, 1998.

Ciccioli, P., Centritto, M., and Loreto, F.: Biogenic volatile organic compound emissions from vegetation fires, Plant Cell Environ., 37, 1810–1825, https://doi.org/10.1111/pce.12336, 2014.

Claeys, M., Graham, B., Vas, G., Wang, W., Vermeylen, R., Pashynska, V., Cafmeyer, J., Guyon, P., Andreae, M. O., Artaxo, P., and Maenhaut, W.: Formation of secondary organic aerosols through photooxidation of isoprene, Science, 303, 1173–1176, https://doi.org/10.1126/science.1092805, 2004a.

Claeys, M., Wang, W., Ion, A. C., Kourtchev, I., Gelencsér, A., and Maenhaut, W.: Formation of secondary organic aerosols from isoprene and its gas-phase oxidation products through reaction with hydrogen peroxide, Atmos. Environ., 38, 4093–4098, https://doi.org/10.1016/j.atmosenv.2004.06.001, 2004b.

Claeys, M., Szmigielski, R., Kourtchev, I., Van der Veken, P., Vermeylen, R., Maenhaut, W., Jaoui, M., Kleindienst, T. E., Lewandowski, M., Offenberg, J. H., and Edney, E. O.: Hydroxydicarboxylic acids:? Markers for secondary organic aerosol from the photooxidation of α-pinene, Environ. Sci. Technol., 41, 1628–1634, https://doi.org/10.1021/es0620181, 2007.

Cui, T., Zeng, Z., dos Santos, E. O., Zhang, Z., Chen, Y., Zhang, Y., Rose, C. A., Budisulistiorini, S. H., Collins, L. B., Bodnar, W. M., de Souza, R. A. F., Martin, S. T., Machado, C. M. D., Turpin, B. J., Gold, A., Ault, A. P., and Surratt, J. D.: Development of a hydrophilic interaction liquid chromatography (HILIC) method for the chemical characterization of water-soluble isoprene epoxydiol (IEPOX)-derived secondary organic aerosol, Environ. Sci.: Process. Imp., 20, 1524–1536, https://doi.org/10.1039/C8EM00308D, 2018.

Ding, X., Zheng, M., Yu, L., Zhang, X., Weber, R. J., Yan, B., Russell, A. G., Edgerton, E. S., and Wang, X.: Spatial and seasonal trends in biogenic secondary organic aerosol tracers and water-soluble organic carbon in the southeast-ern United States, Environ. Sci. Technol., 42, 5171–5176, https://doi.org/10.1021/es7032636, 2008.

Ding, X., Wang, X., and Zheng, M.: The influence of temperature and aerosol acidity on biogenic secondary organic aerosol tracers: Observations at a rural site in the central Pearl River Delta region, South China, Atmos. Environ., 45, 1303–1311, https://doi.org/10.1016/j.atmosenv.2010.11.057, 2011.

Ding, X., Wang, X., Gao, B., Fu, X., He, Q., Zhao, X., Yu, J., and Zheng, M.: Tracer based estimation of secondary organic carbon in the Pearl River Delta, South China, J. Geophys. Res.-Atmos., 117, D05313, https://doi.org/10.1029/2011JD016596, 2012.

Ding, X., Wang, X., Xie, Z., Zhang, Z., and Sun, L.: Impacts of Siberian biomass burning on organic aerosols over the North Pacific Ocean and the Arctic: Primary and secondary organic tracers, Environ. Sci. Technol., 47, 3149–3157, https://doi.org/10.1021/es3037093, 2013.

Ding, X., He, Q. F., Shen, R. Q., Yu, Q. Q., and Wang, X. M.: Spatial distributions of secondary organic aerosols from isoprene, monoterpenes, β-caryophyllene, and aromatics over China during summer, J. Geophys. Res.-Atmos., 119, 11877–11891, https://doi.org/10.1002/2014JD021748, 2014.

Ding, X., He, Q. F., Shen, R. Q., Yu, Q. Q., Zhang, Y. Q., Xin, J. Y., Wen, T. X., and Wang, X. M.: Spatial and seasonal variations of isoprene secondary organic aerosol in China: Significant impact of biomass burning during winter, Sci. Rep., 6, 20411, https://doi.org/10.1038/srep20411, 2016a.

Ding, X., Zhang, Y. Q., He, Q. F., Yu, Q. Q., Shen, R. Q., Zhang, Y., Zhang, Z., Lyu, S. J., Hu, Q. H., Wang, Y. S., Li, L. F., Song, W., and Wang, X. M.: Spatial and seasonal variations of secondary organic aerosol from terpenoids over China, J. Geophys. Res.-Atmos., 121, 14661–14678, https://doi.org/10.1002/2016JD025467, 2016b.

Donahue, N. M., Robinson, A. L., Stanier, C. O., and Pandis, S. N.: Coupled partitioning, dilution, and chemical aging of semivolatile organics, Environ. Sci. Technol., 40, 2635–2643, https://doi.org/10.1021/es052297c, 2006.

Eddingsaas, N. C., Loza, C. L., Yee, L. D., Chan, M., Schilling, K. A., Chhabra, P. S., Seinfeld, J. H., and Wennberg, P. O.: α-pinene photooxidation under controlled chemical conditions – Part 2: SOA yield and composition in low- and high-NO$_x$ environments, Atmos. Chem. Phys., 12, 7413–7427, https://doi.org/10.5194/acp-12-7413-2012, 2012.

Guenther, A. B., Jiang, X., Heald, C. L., Sakulyanontvittaya, T., Duhl, T., Emmons, L. K., and Wang, X.: The Model of Emissions of Gases and Aerosols from Nature version 2.1 (MEGAN2.1): an extended and updated framework for modeling biogenic emissions, Geosci. Model Dev., 5, 1471–1492, https://doi.org/10.5194/gmd-5-1471-2012, 2012.

Haque, M. M., Kawamura, K., and Kim, Y.: Seasonal variations of biogenic secondary organic aerosol tracers in ambient aerosols from Alaska, Atmos. Environ., 130, 95–104, https://doi.org/10.1016/j.atmosenv.2015.09.075, 2016.

He, M., Zheng, J., Yin, S., and Zhang, Y.: Trends, temporal and spatial characteristics, and uncertainties in biomass burning emissions in the Pearl River Delta, China, Atmos. Environ., 45, 4051–4059, https://doi.org/10.1016/j.atmosenv.2011.04.016, 2011.

He, Q. F., Ding, X., Wang, X. M., Yu, J. Z., Fu, X. X., Liu, T. Y., Zhang, Z., Xue, J., Chen, D. H., Zhong, L. J., and Donahue, N. M.: Organosulfates from pinene and isoprene over the Pearl

River Delta, South China: Seasonal variation and implication in formation mechanisms, Environ. Sci. Technol., 48, 9236–9245, https://doi.org/10.1021/es501299v, 2014.

He, Q. F., Ding, X., Fu, X. X., Zhang, Y. Q., Wang, J. Q., Liu, Y. X., Tang, M. J., Wang, X. M., and Rudich, Y.: Secondary organic aerosol formation from isoprene epoxides in the Pearl River Delta, South China: IEPOX- and HMML-derived tracers, J. Geophys. Res.-Atmos., 123, 6999–7012, https://doi.org/10.1029/2017JD028242, 2018.

Hofzumahaus, A., Rohrer, F., Lu, K., Bohn, B., Brauers, T., Chang, C.-C., Fuchs, H., Holland, F., Kita, K., Kondo, Y., Li, X., Lou, S., Shao, M., Zeng, L., Wahner, A., and Zhang, Y.: Amplified trace gas removal in the troposphere, Science, 324, 1702–1704, https://doi.org/10.1126/science.1164566, 2009.

Hoyle, C. R., Boy, M., Donahue, N. M., Fry, J. L., Glasius, M., Guenther, A., Hallar, A. G., Huff Hartz, K., Petters, M. D., Petäjä, T., Rosenoern, T., and Sullivan, A. P.: A review of the anthropogenic influence on biogenic secondary organic aerosol, Atmos. Chem. Phys., 11, 321–343, https://doi.org/10.5194/acp-11-321-2011, 2011.

Hu, Q. H., Xie, Z. Q., Wang, X. M., Kang, H., He, Q. F., and Zhang, P.: Secondary organic aerosols over oceans via oxidation of isoprene and monoterpenes from Arctic to Antarctic, Sci. Rep., 3, 2280, https://doi.org/10.1038/srep02280, 2013.

Jaoui, M., Lewandowski, M., Kleindienst, T. E., Offenberg, J. H., and Edney, E. O.: β-caryophyllinic acid: An atmospheric tracer for β-caryophyllene secondary organic aerosol, Geophys. Res. Let., 34, L05816, https://doi.org/10.1029/2006gl028827, 2007.

Keeling, C. I. and Bohlmann, J.: Genes, enzymes and chemicals of terpenoid diversity in the constitutive and induced defence of conifers against insects and pathogens, New Phytol., 170, 657–675, https://doi.org/10.1111/j.1469-8137.2006.01716.x, 2006.

Kleindienst, T. E., Jaoui, M., Lewandowski, M., Offenberg, J. H., Lewis, C. W., Bhave, P. V., and Edney, E. O.: Estimates of the contributions of biogenic and anthropogenic hydrocarbons to secondary organic aerosol at a southeastern US location, Atmos. Environ., 41, 8288–8300, https://doi.org/10.1016/j.atmosenv.2007.06.045, 2007.

Lai, C., Liu, Y., Ma, J., Ma, Q., Chu, B., and He, H.: Heterogeneous kinetics of cis-pinonic acid with hydroxyl radical under different environmental conditions, J. Phys. Chem. A., 119, 6583–6593, https://doi.org/10.1021/acs.jpca.5b01321, 2015.

Lewandowski, M., Piletic, I. R., Kleindienst, T. E., Offenberg, J. H., Beaver, M. R., Jaoui, M., Docherty, K. S., and Edney, E. O.: Secondary organic aerosol characterisation at field sites across the United States during the spring–summer period, Int. J. Environ. An. Ch., 93, 1084–1103, https://doi.org/10.1080/03067319.2013.803545, 2013.

Li, J., Wang, G., Wu, C., Cao, C., Ren, Y., Wang, J., Li, J., Cao, J., Zeng, L., and Zhu, T.: Characterization of isoprene-derived secondary organic aerosols at a rural site in North China Plain with implications for anthropogenic pollution effects, Sci. Rep., 8, 535, https://doi.org/10.1038/s41598-017-18983-7, 2018.

Lin, Y.-H., Zhang, Z., Docherty, K. S., Zhang, H., Budisulistiorini, S. H., Rubitschun, C. L., Shaw, S., Knipping, E., Edgerton, E. S., Kleindienst, T. E., Gold, A., and Surratt, J. D.: Isoprene epoxydiols as precursors to secondary organic aerosol formation: Acid-catalyzed reactive uptake studies with authentic standards, Environ. Sci. Technol., 46, 189–195, https://doi.org/10.1021/es202554c, 2012.

Lopez-Hilfiker, F. D., Mohr, C., D'Ambro, E. L., Lutz, A., Riedel, T. P., Gaston, C. J., Iyer, S., Zhang, Z., Gold, A., Surratt, J. D., Lee, B. H., Kurten, T., Hu, W. W., Jimenez, J., Hallquist, M., and Thornton, J. A.: Molecular composition and volatility of organic aerosol in the southeastern U.S.: Implications for IEPOX derived SOA, Environ. Sci. Technol., 50, 2200–2209, https://doi.org/10.1021/acs.est.5b04769, 2016.

Lu, Q., Zheng, J., Ye, S., Shen, X., Yuan, Z., and Yin, S.: Emission trends and source characteristics of SO_2, NO_x, PM_{10} and VOCs in the Pearl River Delta region from 2000 to 2009, Atmos. Environ., 76, 11–20, https://doi.org/10.1016/j.atmosenv.2012.10.062, 2013.

Mentel, Th. F., Kleist, E., Andres, S., Dal Maso, M., Hohaus, T., Kiendler-Scharr, A., Rudich, Y., Springer, M., Tillmann, R., Uerlings, R., Wahner, A., and Wildt, J.: Secondary aerosol formation from stress-induced biogenic emissions and possible climate feedbacks, Atmos. Chem. Phys., 13, 8755–8770, https://doi.org/10.5194/acp-13-8755-2013, 2013.

Müller, L., Reinnig, M.-C., Naumann, K. H., Saathoff, H., Mentel, T. F., Donahue, N. M., and Hoffmann, T.: Formation of 3-methyl-1,2,3-butanetricarboxylic acid via gas phase oxidation of pinonic acid – a mass spectrometric study of SOA aging, Atmos. Chem. Phys., 12, 1483–1496, https://doi.org/10.5194/acp-12-1483-2012, 2012.

Nguyen, T. B., Bates, K. H., Crounse, J. D., Schwantes, R. H., Zhang, X., Kjaergaard, H. G., Surratt, J. D., Lin, P., Laskin, A., Seinfeld, J. H., and Wennberg, P. O.: Mechanism of the hydroxyl radical oxidation of methacryloyl peroxynitrate (MPAN) and its pathway toward secondary organic aerosol formation in the atmosphere, Phys. Chem. Chem. Phys., 17, 17914–17926, https://doi.org/10.1039/C5CP02001H, 2015.

Offenberg, J. H., Lewis, C. W., Lewandowski, M., Jaoui, M., Kleindienst, T. E., and Edney, E. O.: Contributions of toluene and α-pinene to SOA formed in an irradiated toluene/α-pinene/NO_x/air mixture: Comparison of results using ^{14}C content and SOA organic tracer methods, Environ. Sci. Technol., 41, 3972–3976, https://doi.org/10.1021/es070089+, 2007.

Offenberg, J. H., Lewandowski, M., Edney, E. O., Kleindienst, T. E., and Jaoui, M.: Influence of aerosol acidity on the formation of secondary organic aerosol from biogenic precursor hydrocarbons, Environ. Sci. Technol., 43, 7742–7747, https://doi.org/10.1021/es901538e, 2009.

Ou, J., Yuan, Z., Zheng, J., Huang, Z., Shao, M., Li, Z., Huang, X., Guo, H., and Louie, P. K. K.: Ambient ozone control in a photochemically active region: Short-term despiking or long-term attainment?, Environ. Sci. Technol., 50, 5720–5728, https://doi.org/10.1021/acs.est.6b00345, 2016.

Paulot, F., Crounse, J. D., Kjaergaard, H. G., Kürten, A., St. Clair, J. M., Seinfeld, J. H., and Wennberg, P. O.: Unexpected epoxide formation in the gas-phase photooxidation of isoprene, Science, 325, 730–733, https://doi.org/10.1126/science.1172910, 2009.

Pye, H. O. T., Pinder, R. W., Piletic, I. R., Xie, Y., Capps, S. L., Lin, Y.-H., Surratt, J. D., Zhang, Z., Gold, A., Luecken, D. J., Hutzell, W. T., Jaoui, M., Offenberg, J. H., Kleindienst, T. E., Lewandowski, M., and Edney, E. O.: Epoxide pathways improve model predictions of isoprene markers and reveal key role of

acidity in aerosol formation, Environ. Sci. Technol., 47, 11056–11064, https://doi.org/10.1021/es402106h, 2013.

Riva, M., Budisulistiorini, S. H., Zhang, Z., Gold, A., and Surratt, J. D.: Chemical characterization of secondary organic aerosol constituents from isoprene ozonolysis in the presence of acidic aerosol, Atmos. Environ., 130, 5–13, https://doi.org/10.1016/j.atmosenv.2015.06.027, 2016.

Riva, M., Budisulistiorini, S. H., Zhang, Z., Gold, A., Thornton, J. A., Turpin, B. J., and Surratt, J. D.: Multiphase reactivity of gaseous hydroperoxide oligomers produced from isoprene ozonolysis in the presence of acidified aerosols, Atmos. Environ., 152, 314–322, https://doi.org/10.1016/j.atmosenv.2016.12.040, 2017.

Shen, R.-Q., Ding, X., He, Q.-F., Cong, Z.-Y., Yu, Q.-Q., and Wang, X.-M.: Seasonal variation of secondary organic aerosol tracers in Central Tibetan Plateau, Atmos. Chem. Phys., 15, 8781–8793, https://doi.org/10.5194/acp-15-8781-2015, 2015.

Sipilä, M., Jokinen, T., Berndt, T., Richters, S., Makkonen, R., Donahue, N. M., Mauldin III, R. L., Kurtén, T., Paasonen, P., Sarnela, N., Ehn, M., Junninen, H., Rissanen, M. P., Thornton, J., Stratmann, F., Herrmann, H., Worsnop, D. R., Kulmala, M., Kerminen, V.-M., and Petäjä, T.: Reactivity of stabilized Criegee intermediates (sCIs) from isoprene and monoterpene ozonolysis toward SO_2 and organic acids, Atmos. Chem. Phys., 14, 12143–12153, https://doi.org/10.5194/acp-14-12143-2014, 2014.

St. Clair, J. M., Rivera-Rios, J. C., Crounse, J. D., Knap, H. C., Bates, K. H., Teng, A. P., Jørgensen, S., Kjaergaard, H. G., Keutsch, F. N., and Wennberg, P. O.: Kinetics and products of the reaction of the first-generation isoprene hydroxy hydroperoxide (ISOPOOH) with OH, J. Phys. Chem. A., 120, 1441–1451, https://doi.org/10.1021/acs.jpca.5b06532, 2016.

Stone, E. A., Nguyen, T. T., Pradhan, B. B., and Man Dangol, P.: Assessment of biogenic secondary organic aerosol in the Himalayas, Environ. Chem., 9, 263–272, https://doi.org/10.1071/EN12002, 2012.

Surratt, J. D., Chan, A. W. H., Eddingsaas, N. C., Chan, M., Loza, C. L., Kwan, A. J., Hersey, S. P., Flagan, R. C., Wennberg, P. O., and Seinfeld, J. H.: Reactive intermediates revealed in secondary organic aerosol formation from isoprene, P. Natl. Acad. Sci. USA, 107, 6640–6645, https://doi.org/10.1073/pnas.0911114107, 2010.

Szmigielski, R., Surratt, J. D., Gómez-González, Y., Van der Veken, P., Kourtchev, I., Vermeylen, R., Blockhuys, F., Jaoui, M., Kleindienst, T. E., Lewandowski, M., Offenberg, J. H., Edney, E. O., Seinfeld, J. H., Maenhaut, W., and Claeys, M.: 3-methyl-1,2,3-butanetricarboxylic acid: An atmospheric tracer for terpene secondary organic aerosol, Geophys. Res. Lett., 34, L24811, https://doi.org/10.1029/2007gl031338, 2007.

Von Schneidemesser, E., Monks, P. S., Allan, J. D., Bruhwiler, L., Forster, P., Fowler, D., Lauer, A., Morgan, W. T., Paasonen, P., Righi, M., Sindelarova, K., and Sutton, M. A.: Chemistry and the linkages between air quality and climate change, Chem. Rev., 115, 3856–3897, https://doi.org/10.1021/acs.chemrev.5b00089, 2015.

Wang, W., Kourtchev, I., Graham, B., Cafmeyer, J., Maenhaut, I., and Claeys, M.: Characterization of oxygenated derivatives of isoprene related to 2-methyltetrols in Amazonian aerosols using trimethylsilylation and gas chromatography/ion trap mass spectrometry, Rapid Commun. Mass Spectrom., 19, 1343–1351, https://doi.org/10.1002/rcm.1940, 2005.

Wang, X., Liu, H., Pang, J., Carmichael, G., He, K., Fan, Q., Zhong, L., Wu, Z., and Zhang, J.: Reductions in sulfur pollution in the Pearl River Delta region, China: Assessing the effectiveness of emission controls, Atmos. Environ., 76, 113–124, https://doi.org/10.1016/j.atmosenv.2013.04.074, 2013.

Watanabe, A. C., Stropoli, S. J., and Elrod, M. J.: Assessing the potential mechanisms of isomerization reactions of isoprene epoxydiols on secondary organic aerosol, Environ. Sci. Technol., 52, 8346–8354, https://doi.org/10.1021/acs.est.8b01780, 2018.

Worton, D. R., Surratt, J. D., LaFranchi, B. W., Chan, A. W. H., Zhao, Y., Weber, R. J., Park, J.-H., Gilman, J. B., de Gouw, J., Park, C., Schade, G., Beaver, M., Clair, J. M. S., Crounse, J., Wennberg, P., Wolfe, G. M., Harrold, S., Thornton, J. A., Farmer, D. K., Docherty, K. S., Cubison, M. J., Jimenez, J.-L., Frossard, A. A., Russell, L. M., Kristensen, K., Glasius, M., Mao, J., Ren, X., Brune, W., Browne, E. C., Pusede, S. E., Cohen, R. C., Seinfeld, J. H., and Goldstein, A. H.: Observational insights into aerosol formation from isoprene, Environ. Sci. Technol., 47, 11396–11402, https://doi.org/10.1021/es4011064, 2013.

Xu, L., Guo, H., Boyd, C. M., Klein, M., Bougiatioti, A., Cerully, K. M., Hite, J. R., Isaacman-VanWertz, G., Kreisberg, N. M., Knote, C., Olson, K., Koss, A., Goldstein, A. H., Hering, S. V., de Gouw, J., Baumann, K., Lee, S.-H., Nenes, A., Weber, R. J., and Ng, N. L.: Effects of anthropogenic emissions on aerosol formation from isoprene and monoterpenes in the southeastern United States, P. Natl. Acad. Sci. USA, 112, 37–42, https://doi.org/10.1073/pnas.1417609112, 2015.

Xu, L., Middlebrook, A. M., Liao, J., de Gouw, J. A., Guo, H., Weber, R. J., Nenes, A., Lopez-Hilfiker, F. D., Lee, B. H., Thornton, J. A., Brock, C. A., Neuman, J. A., Nowak, J. B., Pollack, I. B., Welti, A., Graus, M., Warneke, C., and Ng, N. L.: Enhanced formation of isoprene-derived organic aerosol in sulfur-rich power plant plumes during Southeast Nexus, J. Geophys. Res.-Atmos., 121, 11137–11153, https://doi.org/10.1002/2016JD025156, 2016.

Ye, J., Abbatt, J. P. D., and Chan, A. W. H.: Novel pathway of SO_2 oxidation in the atmosphere: reactions with monoterpene ozonolysis intermediates and secondary organic aerosol, Atmos. Chem. Phys., 18, 5549–5565, https://doi.org/10.5194/acp-18-5549-2018, 2018.

Zhang, R. Y., Wang, G. H., Guo, S., Zarnora, M. L., Ying, Q., Lin, Y., Wang, W. G., Hu, M., and Wang, Y.: Formation of urban fine particulate matter, Chem. Rev., 115, 3803–3855, https://doi.org/10.1021/acs.chemrev.5b00067, 2015.

Zheng, J., Zheng, Z., Yu, Y., and Zhong, L.: Temporal, spatial characteristics and uncertainty of biogenic VOC emissions in the Pearl River Delta region, China, Atmos. Environ., 44, 1960–1969, https://doi.org/10.1016/j.atmosenv.2010.03.001, 2010.